



Oxazole Derivatives as Corrosion Inhibitors for 316L Stainless Steel in Sulfamic Acid Solutions

Fouda A.S.^{1*}, Elmorsi M.A.², Fayed T.² and El said M.¹

¹Department of Chemistry, Faculty of Science, El-Mansoura University, El-Mansoura-35516, EGYPT

²Department of Chemistry, Faculty of Science, Tanta University, Tanta, EGYPT

Available online at: www.isca.in, www.isca.me

Received 3rd August 2014, revised 12th August 2014, accepted 17th August 2014

Abstract

Oxazole derivatives were investigated as corrosion inhibitors for 316L stainless steel (SS) in sulfamic acid (NH_2HSO_3) solutions by potentiodynamic polarization, electrochemical impedance spectroscopy (EIS) and electrochemical frequency modulation (EFM) techniques. The results showed the variation in inhibition performance of the inhibitors with varying concentrations and temperatures. The maximum efficiency was found to be 91% at 2×10^{-4} M concentration of the inhibitors for the immersion period of 3 hours. Langmuir was tested to describe the adsorption behavior of inhibitor on 316L SS surface. Potentiodynamic polarization study clearly revealed that these compounds act as mixed type inhibitors. The results of the electrochemical impedance study showed a decrease in double layer capacitance and increase in charge transfer resistance. The results of various electrochemical techniques show good agreements with each other.

Keywords: Corrosion inhibition, stainless steel, sulfamic acid, potentiodynamic polarization, EIS, EFM

Introduction

Sulfamic acid (amido sulfuric acid) has long been used as an industrial cleaning agent due to its remarkable property of solubilizing hard scales and most of the deposits. Furthermore, it can be used on stainless steels with no problem of pitting or chloride - induced stress corrosion cracking (SCC). Sulfamic acid finds application in desalination plants for cleaning demisters, heat exchangers and cooling water systems. Optimization in the sulfamic acid treatment is desirable in terms of plant efficiency and economic considerations. However, in spite of its capability as a potential descaling and an excellent cleaner, the industrial chemical treatment is somewhat qualitative due to the lack of corrosion and dissolution data regarding sulfamic acid¹. Sulfamic acid behaves as a strong acid in aqueous solution but the corrosion rates are significantly lower in comparison to other acids². The low corrosion rates can be reduced further by the addition of corrosion inhibitors³. It can be used for cleaning stainless steels with no problem of chloride induced stress corrosion cracking. Due to these formidable properties, acid cleaners based on sulfamic acid are extensively used in a large variety of household and industrial applications⁴.

Efficient inhibitors for 316 SS are heterocyclic organic compounds consisting of a π -system and P, S, N, or O heteroatom. It is noticed that the presence of these functional groups and heteroatom in the organic compound molecules improves its action as stainless steel corrosion inhibitor because they enable chemisorptions, such as azoles⁵⁻¹³, amines¹⁴, amino acids¹⁵, organic derivatives also offer special affinity to inhibit

corrosion of various metals in different acidic media¹⁶⁻²⁵ and many others.

In this study the various electrochemical techniques were used to investigate the effect of some oxazole derivatives as corrosion inhibitors for 316L SS in sulfamic acid solution.

Experimental

Materials and solutions: Experiments were performed using 316SS samples with the following composition (weight %): C 0.03%, Mn 2%, P 0.045%, Si 0.75%, Ni 10-14%, Mo 2-3%, Cr 16-18%, S, N 0.1%, S 0.03% and balance Fe. The aggressive solution used was prepared by dilution of analytical reagent grade sulfamic acid with bidistilled water. The stock solution (1×10^{-2} M) of investigated compounds was used to prepare the desired concentrations by dilution with bidistilled water. The concentration range of investigated compounds was $(4-20 \times 10^{-5})$ M.

Electrochemical measurements: Six test pieces of 316SS were cut into $2 \times 2 \times 0.2$ cm. They were abraded with emery papers (a coarse paper was used initially and then progressively finer grades were employed), degreased in acetone, rinsed with bidistilled water and finally dried between two filter papers and weighed. The test pieces were suspended by suitable glass hooks at the edge of the basin, and under the surface of the test solution by about 1 cm. Weight loss measurements were performed for 3 hours at the temperature range from 25 – 55 °C by immersing 316SS pieces into 100 ml acid solution with and without various concentrations of inhibitors. After the specified periods of time, the specimen were taken out of the

Table-1
Composition of 316L SS samples

element	C	Cr	Ni	Mo	Mn	Si	P	S	N	Fe
weight%	0.03	16-18	10-14	2-3	2	0.75	0.045	0.03	0.1	balance

test solution, rinsed with bidistilled water, dried as before and weighed again accurately. The average weight loss at a certain time for each set of the six samples was taken. The weight loss was recorded to nearest 0.0001 g.

Electrochemical measurements: Electrochemical experiments were performed using a typical three-compartment glass cell consisted of the 316SS specimen as working electrode (1 cm²), saturated calomel electrode (SCE) as a reference electrode and a platinum foil (1 cm²) as a counter electrode. The reference electrode was connected to a Luggin capillary and the tip of the Luggin capillary is made very close to the surface of the working electrode to minimize IR drop. All the measurements were done in solutions open to atmosphere under unstirred conditions. All potential values were reported versus SCE. Prior to every experiment, the electrode was abraded with successive different grades of emery paper, degreased with acetone and washed with bidistilled water and finally dried. Tafel polarization curves were obtained by changing the electrode potential automatically from (-1.0 to 0.2 V vs. SCE) at open circuit potential with a scan rate of 1 mVs⁻¹. The corrosion current is performed by extrapolation of anodic and cathodic Tafel lines to a point which gives log i_{corr} and the corresponding corrosion potential (E_{corr}) for inhibitor free acid and for each concentration of inhibitor.

Impedance measurements were carried out in frequency range from 100 kHz to 0.1Hz with amplitude of 5 mV peak-to-peak using ac signals at open circuit potential. The experimental impedance was analyzed and interpreted based on the equivalent

circuit. The main parameters deduced from the analysis of Nyquist diagram are the charge transfer resistance R_{ct} (diameter of high-frequency loop) and the double layer capacity C_{dl} .

Electrochemical frequency modulation, EFM, was carried out using two frequencies 2 and 5 Hz. The base frequency was 0.1 Hz, so the waveform repeats after 1 s. The higher frequency must be at least two times the lower one. The higher frequency must also be sufficiently slow that the charging of the double layer does not contribute to the current response. Often, 10 Hz is a reasonable limit. The Intermodulation spectra contain current responses assigned for harmonical and intermodulation current peaks. The larger peaks were used to calculate the corrosion current density (i_{corr}), the Tafel slopes (β_c and β_a) and the causality factors CF-2 and CF-3

All electrochemical measurements were performed using Gamry Instrument (PCI 300/4) Potentiostat / Galvanostat / ZRA. This includes a Gamry framework system based on the ESA 400. Gamry applications include DC105 software for potentiodynamic polarization measurements, EIS300 software for electrochemical impedance spectroscopy and EFM 140 software for electrochemical frequency modulation measurements along with a computer for collecting data. Echem Analyst 6.03 software was used for plotting, graphing, and fitting data.

To test the reliability and reproducibility of the measurements, duplicate experiments were performed in each case at the same conditions.

Table-2
Chemical structures, names, molecular weights and molecular formulas of oxazole derivatives

Inhibitor	Structures	Names	Molecular weights	Chemical formulas
A		(E)-2-styrylbenzo[d]oxazole	221.25	C ₁₅ H ₁₁ NO
B		(E)-2-(2-(naphthalene-2-yl)vinyl)benzo[d]oxazole	271.31	C ₁₉ H ₁₃ NO
C		(E)-2-(2-(phenanthren-2-yl)vinyl)benzo[d]oxazole	321.37	C ₂₃ H ₁₅ NO
D		(E)-2-(2-(pyren-2-yl)vinyl)benzo[d]oxazole	345.39	C ₂₅ H ₁₅ NO

Results and Discussion

Weight loss method: Figure-1 shows plots for the variation of weight loss of 316L SS with time for the corrosion of SS in 0.6M NH₂HSO₃ containing various concentrations of compound (D) at 25°C. Similar curves were obtained for other inhibitor but not shown. From the plots, it is evident that the weight loss of SS was also found to decrease with increase in the concentration of compound (D). The weight loss of SS in the blank solution was also found to be higher than those obtained for solutions of NH₂HSO₃ containing various concentrations of compound (D). These indicate that compound D is an adsorption inhibitor for the corrosion of SS in solutions of NH₂HSO₃. In table-3, values of the corrosion rates of SS and inhibition efficiency of all studied compounds in various media

are presented. The degree of surface coverage (θ) and inhibition efficiency (% IE) were calculated using equation (1):

$$\% \text{ IE} = \theta \times 100 = [1 - \text{CR}_{\text{inh}} / \text{CR}_{\text{free}}] \times 100 \quad (1)$$

Where CR_{inh} and CR_{free} are the corrosion rates in the absence and presence of inhibitor, respectively. It can be seen that the maximum of 90.6% inhibition efficiency is achieved at 2 x 10⁻⁴ M of inhibitor concentration and %IE increases with increasing the inhibitors concentrations²⁶. This is mainly due to the active chemical constituent of viz, π bonds, hetero atoms (O and N). The almost greater than 90% of surface coverage (θ) is due to the co-ordination between the metal and the hetero atom present in the inhibitor. From the calculated values of %IE, the order of the inhibition efficiency of inhibitors was as follows: D > B > A > C.

Table-3
Corrosion Rate (C.R.) and inhibition efficiency (%IE) at different concentrations of inhibitors for the corrosion of 316L SS after 120 min immersion in 0.6 M NH₂HSO₃ at 25°C

Conc., x 10 ⁵ M	A		B		C		D	
	C.R. x10 ³ mg cm ⁻² min ⁻¹	%IE	C.R. x10 ³ mg cm ⁻² min ⁻¹	%IE	C.R. x10 ³ mg cm ⁻² min ⁻¹	%IE	C.R. x10 ³ mg cm ⁻² min ⁻¹	%IE
4.0	3.24	72.4	3.47	70.5	4.07	65.4	2.91	75.2
8.0	2.63	77.6	2.82	76.0	3.28	72.0	2.17	81.5
12	2.12	81.9	2.12	81.9	2.59	78.0	1.66	85.8
16	1.66	85.8	1.43	87.8	2.17	81.5	1.38	88.2
20	1.48	87.4	1.25	89.4	1.89	83.9	1.11	90.6

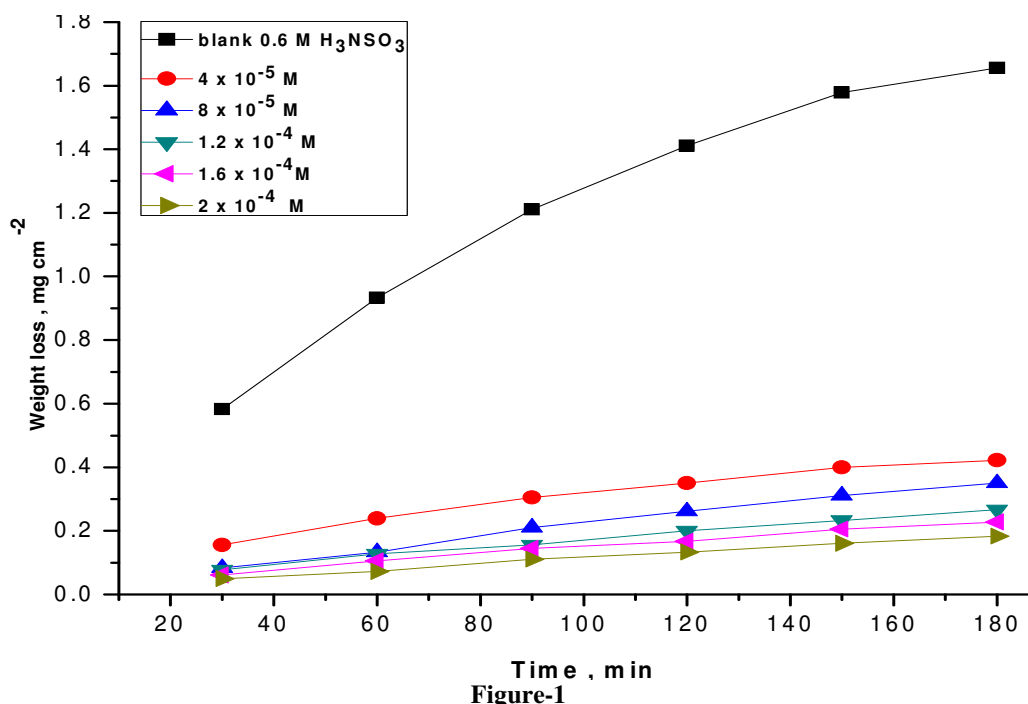


Figure-1
Weight loss-time curves for the corrosion of 316SS in 0.6 M NH₂HSO₃ in the absence and presence of different concentrations of inhibitor (D) at 25°C

Effect of temperature on inhibition efficiency (% IE): The inhibition efficiency (% IE) for 316SS corrosion in the presence of various concentrations of the investigated oxazole derivatives and at different temperatures was calculated and is listed in table-4. The results of table-4 illustrate the variation of corrosion rate (C.R.) and %IE with inhibitors concentrations at different temperatures. The obtained data revealed that, the inhibition efficiency decreased with an increase in the inhibitor concentration. This suggests that the inhibitor species are adsorbed on the 316SS /solution interface where the adsorbed species mechanically form a protected film on the metal surface which inhibits the action of the corrosion. A close comparison between tables 2 and 3 revealed that weight loss of SS increases with increasing temperature indicating that the rate of corrosion of SS increases with increase in temperature. The value of inhibition efficiency was decreased with rise in temperature suggests that physical adsorption mechanism²⁸. These results indicate that the adsorption of investigated compounds shield the metal surface at room temperature²⁹. However it may be de-shielded from the surface with rise in temperature. It is also clear that corrosion rate of 316SS in the absence and presence of inhibitors obeys Arrhenius type equation as it increases with raising solution temperature. The dependence of corrosion rate (k_{corr}) on the temperature can be expressed by Arrhenius equation 2:

$$i_{corr} = A \exp(-E_a^*/RT) \quad (2)$$

where A is the pre-exponential factor and E_a^* is the apparent activation energy of the corrosion process. Arrhenius plot obtained for the corrosion of carbon steel in 0.5 M sulfamic acid solutions in the presence of different concentrations of

compound (D) is shown in figure-2. E_a^* values determined from the slopes of these linear plots are shown in table-5. The linear regression (R^2) is close to 1 which indicates that the corrosion of 316 SS in 0.5 M sulfamic acid solutions can be elucidated using the kinetic model. Table-5 showed that the values of E_a^* for inhibited solution is higher than that for uninhibited solution, suggesting that dissolution of 316 SS is slow in the presence of inhibitor. It is known from Eq. 2 that the higher E_a^* values lead to the lower corrosion rate. This is due to the formation of a film on the carbon steel surface serving as an energy barrier for the carbon steel corrosion³⁰.

Enthalpy and entropy of activation (ΔH^* , ΔS^*) of the corrosion process were calculated from the transition state theory as given from equation 3 (table-4):

$$k_{corr} = (RT/Nh) \exp(\Delta S^*/R) \exp(-\Delta H^*/RT) \quad (3)$$

where h is Planck's constant and N is Avogadro's number. A plot of $\log(k_{corr}/T)$ vs. $1/T$ for carbon steel in 0.5 M sulfamic acid with different concentrations of compound (D) gives straight lines as shown in figure-3. Similar curves were obtained for other compounds but not shown. Values of ΔH^* are positive. This indicates that the corrosion process is an endothermic one. The entropy of activation ΔS^* is large and negative. This implies that the activated complex represents association rather than dissociation step, indicating that a decrease in disorder takes place, going from reactants to the activated complex³¹.

Table-4
Variation of inhibition efficiency (%IE) and corrosion Rate (C.R.) for various concentrations of the studied inhibitors at different temperatures

Temp. °C	Conc. x 10 ⁵ M	A		B		C		D	
		C.R. x 10 ⁻³ mg cm ⁻² min ⁻¹	%IE	C.R. x 10 ⁻³ mg cm ⁻² min ⁻¹	%IE	C.R. x 10 ⁻³ mg cm ⁻² min ⁻¹	%IE	C.R. x 10 ⁻³ mg cm ⁻² min ⁻¹	%IE
35	4	8.28	66.5	8.05	67.5	9.02	63.5	7.407	70.1
	8	6.66	73.1	6.57	73.5	7.59	69.3	5.324	78.5
	12	5.23	78.9	5.32	78.5	6.43	74.0	3.98	83.9
	16	4.62	81.3	3.98	83.9	5.41	78.1	3.37	86.4
	20	3.75	84.9	2.91	88.2	4.58	81.5	2.73	89.0
45	4	17.87	65.3	17.68	65.6	18.84	63.4	15.55	69.8
	8	14.72	71.4	15.00	70.9	17.26	66.5	11.48	77.7
	12	12.17	76.3	12.08	76.5	14.63	71.5	8.70	83.1
	16	10.41	79.8	8.51	83.5	12.54	75.6	7.59	85.3
	20	9.35	81.8	7.45	85.5	10.92	78.8	6.20	88.0
55	4	37.31	63.3	38.05	62.5	44.30	65.4	31.29	69.2
	8	31.11	69.4	32.22	68.3	36.08	63.8	24.21	76.2
	12	26.34	74.1	26.11	74.3	31.20	69.3	19.07	81.2
	16	23.75	76.6	19.02	81.3	26.89	73.5	16.20	84.0
	20	21.76	78.6	16.29	83.9	24.21	76.2	13.28	78.0

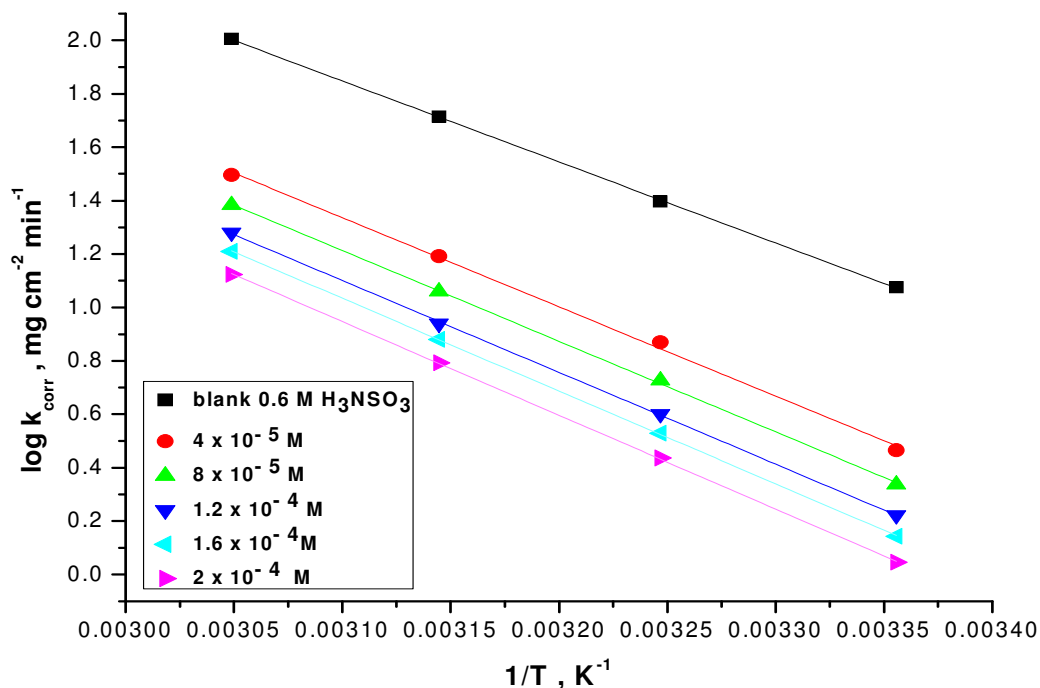


Figure-2

Arrhenius plots for 316SS rates (k_{corr}) after 120 min. immersion in 0.6 M H_2NHSO_3 in the absence and presence of various concentrations of inhibitor (D)

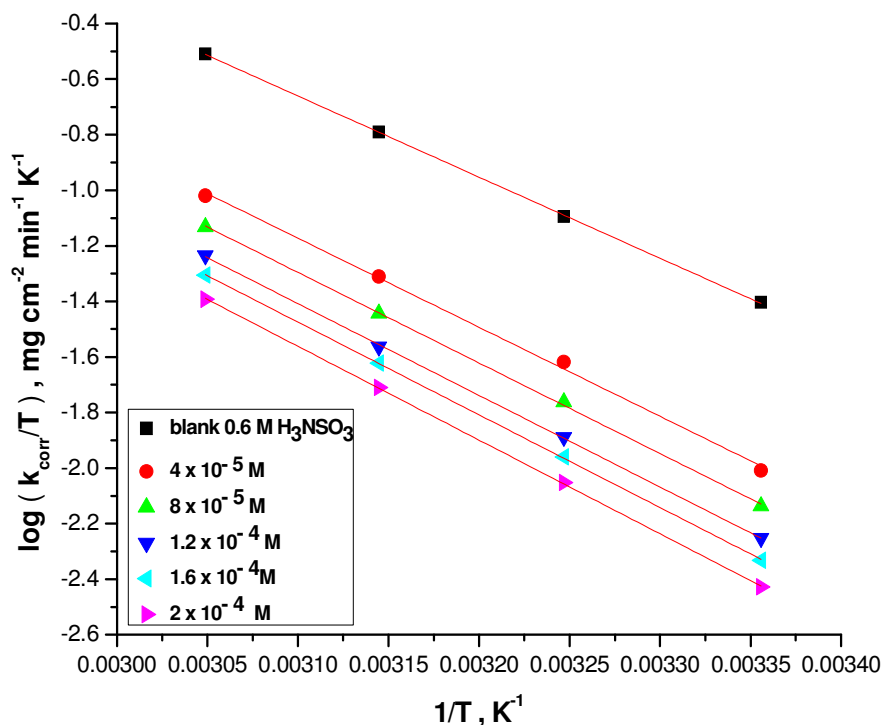


Figure-3

Transition state plots for 316SS (k_{corr}/T vs $1/T$) after 120 min. immersion in 0.6 M H_2NHSO_3 in the absence and presence of various concentrations of compound (D)

Adsorption isotherms: Adsorption isotherm values are important to explain the mechanism of corrosion inhibition of organo-electrochemical reactions. The most frequently used isotherms are Langmuir isotherm (figure-2). Thermodynamic parameters for the adsorption of different inhibitors on 316SS surface in 0.6 M H₂NHSO₃ at different temperatures was listed in table -6.

Table-5
Activation parameters for 316SS surface corrosion in the absence and presence of various concentrations of investigated inhibitors in 0.6 M H₂NHSO₃

Inhibitor	Conc. x 10 ⁵ M	Activation parameters		
		E _a [*] kJ mol ⁻¹	ΔH [*] kJ mol ⁻¹	-ΔS [*] J mol ⁻¹ K ⁻¹
Blank	0.0	58.1	55.9	36.9
A	4	65.9	63.3	22.5
	8	66.6	64.0	21.7
	12	68.2	65.6	18.4
	16	71.4	68.8	9.4
	20	72.9	70.3	5.7
B	4	64.7	62.1	26.0
	8	66.0	63.4	23.4
	12	67.8	65.6	18.4
	16	69.2	66.7	17.8
	20	70.2	67.6	16.3
C	4	64.1	61.5	27.1
	8	65.6	63.0	23.7
	12	67.1	64.8	19.5
	16	68.2	65.6	18.3
	20	69.1	66.5	16.4
D	4	64.0	61.4	29.7
	8	65.0	62.4	28.8
	12	65.8	63.2	28.6
	16	66.5	63.9	27.6
	20	67.2	64.6	27.2

Table-6
Thermodynamic adsorption parameters for the adsorption of oxazole derivatives on carbon steel in 0.6 M sulfamic acid at different temperatures

Inhibitor	Temp. °C	K _{ads} M ⁻¹	-ΔG _{ads} [*] kJ mol ⁻¹	-ΔH _{ads} [*] kJ mol ⁻¹	-ΔS _{ads} [*] J mol ⁻¹ K ⁻¹
A	25	28.04	18.21	22.38	61.04
	35	22.16	18.22	22.38	59.09
	45	16.73	18.07	22.38	56.75
	55	12.26	17.79	22.38	54.17
B	25	40.18	19.10	15.16	64.06
	35	33.22	19.25	15.16	62.48
	45	26.51	19.29	15.16	60.60
	55	23.28	19.53	15.16	59.53
C	25	21.11	17.51	15.91	58.70
	35	16.58	17.48	15.91	56.70
	45	12.70	17.34	15.91	54.48
	55	12.05	17.74	15.91	54.04
D	25	40.42	19.12	10.81	64.12
	35	35.31	19.42	10.81	63.00
	45	30.70	19.68	10.81	61.84
	55	27.18	19.96	10.81	60.83

From table-6 it was found that the negative values of ΔG_{ads}° reflect that the adsorption of studied oxazole derivatives on 316SS in 0.6 M H_2NHSO_3 solution is spontaneous process³². G_{ads}° values increase (become less negative) with an increase of temperature which indicates the occurrence of exothermic process at which adsorption was unfavorable with increasing reaction temperature as the result of the inhibitor desorption from the stainless steel surface³³. It is usually accepted that the value of ΔG_{ads}° around -20 kJ mol^{-1} or lower indicates the electrostatic interaction between charged metal surface and charged organic molecules in the bulk of the solution³⁴. The negative sign of ΔH_{ads}° reveals that the adsorption of inhibitor molecules is an exothermic process. Generally, an exothermic adsorption process suggests either physisorption or chemisorption while endothermic process is attributed to

chemisorptions³⁵. Generally, enthalpy values up to 41.9 kJ mol^{-1} are related to the electrostatic interactions between charged molecules and charged metal (physisorption) while those around 100 kJ mol^{-1} or higher are attributed to chemisorption. The unshared electron pairs in investigated molecules may interact with d-orbitals of Fe to provide a protective chemisorbed film³⁶. In the case of investigated compounds, the absolute values of enthalpy are relatively low, approaching those typical of physisorption. The values of ΔS_{ads}° in the presence of investigated compounds are large and negative that is accompanied with exothermic adsorption process³⁷. The experimental data give good curves fitting for the applied adsorption isotherm as the correlation coefficients (R^2) were in the range 0.950-0.997. K_{ads} value decreases with the increase of temperature from 25 to 55 °C.

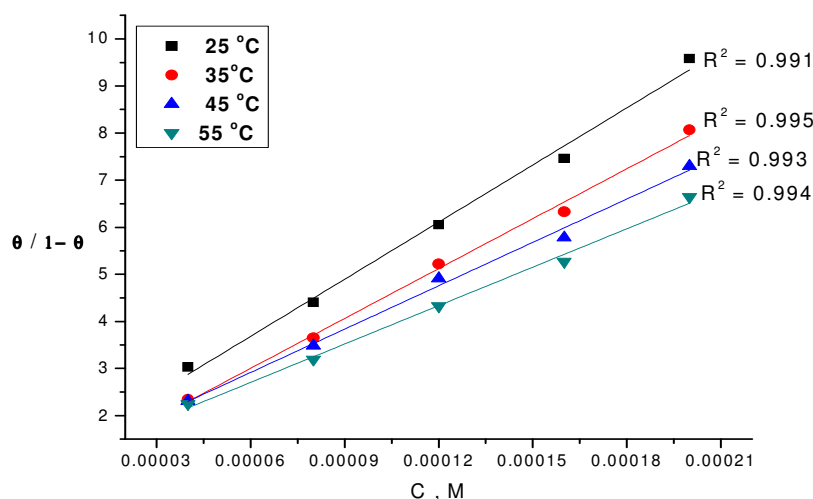


Figure-4
 Langmuir adsorption isotherm of inhibitor (D) on 316SS in 0.6 M H_2NHSO_3 at different temperatures

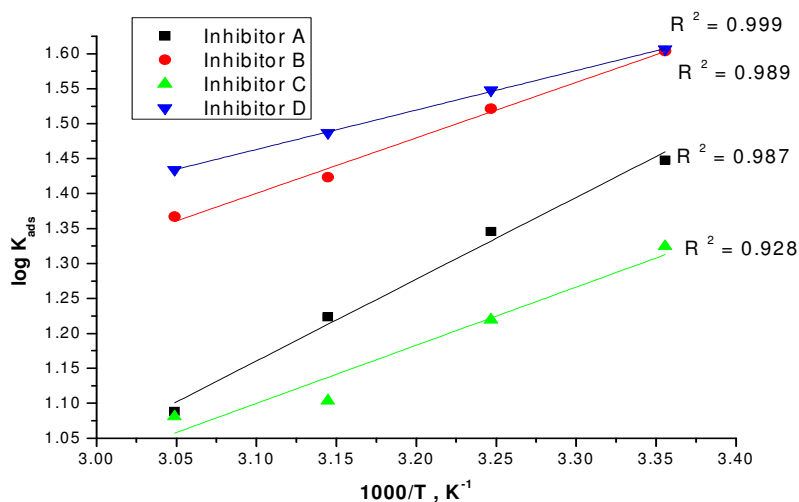


Figure-5
 ($\log K_{ads}$) vs. $(1/T)$ for the corrosion of 316SS in 0.6 M H_2NHSO_3 in the presence of different inhibitors

Potentiodynamic Polarization Measurements: Polarization measurements were carried out in order to gain knowledge concerning the kinetics of the cathodic and anodic reactions. Figure-5 presents the results of the effect of compound (D) on the cathodic and anodic polarization curves of 316SS in 0.6 M H₂NHSO₃. Similar curves for other compounds were obtained but not shown. It could be observed that both the cathodic and anodic reactions were suppressed with the addition of investigated compounds, which suggested that these compounds reduced anodic dissolution and also retarded the hydrogen evolution reaction. Electrochemical corrosion kinetics parameters, i.e. corrosion potential (E_{corr}), cathodic and anodic Tafel slopes (β_a , β_c) and corrosion current density (i_{corr}) obtained from the extrapolation of the polarization curves, were given in table-6. The parallel cathodic Tafel curves in figure-5 suggested that the hydrogen evolution is activation-controlled and the reduction mechanism is not affected by the presence of the inhibitor. The region between linear part of cathodic and anodic branch of polarization curves becomes wider as the inhibitor is added to the acid solution. Similar results were found in the literature³⁸. The values of β_a and β_c changed slightly with increasing inhibitor concentration indicated the influence of these compounds on the kinetics of metal dissolution and of hydrogen evolution. Due to the presence of some active sites, such as aromatic rings, hetero-atoms in the studied compound

for making adsorption, they may act as adsorption inhibitors. Being absorbed on the metal surface, these compounds controlled the anodic and cathodic reactions during corrosion process, and then their corrosion inhibition efficiencies are directly proportional to the amount of adsorbed inhibitor. The functional groups and structure of the inhibitor play important roles during the adsorption process. On the other hand, an electron transfer takes place during adsorption of the neutral organic compounds at metal surface³⁹. As it can be seen from table-6, the studied inhibitor reduced both anodic and cathodic currents with a slight shift in corrosion potential (47 mV). According to Ferreira and others⁴⁰, if the displacement in corrosion potential is more than 85mV with respect to corrosion potential of the blank solution, the inhibitor can be seen as a cathodic or anodic type. In the present study, the displacement was 47 mV which indicated that the studied inhibitor is mixed-type inhibitor. The results obtained from Tafel polarization showed good agreement with the results obtained from weight loss method. The surface coverage (θ) and % IE were calculated using equation 4.

$$\%IE = \theta \times 100 = [1 - (i_{corr}/i_{corr}^{\circ})] \times 100 \quad (4)$$

Where i_{corr} and i_{corr}° are the current densities in presence and absence of inhibitor, respectively.

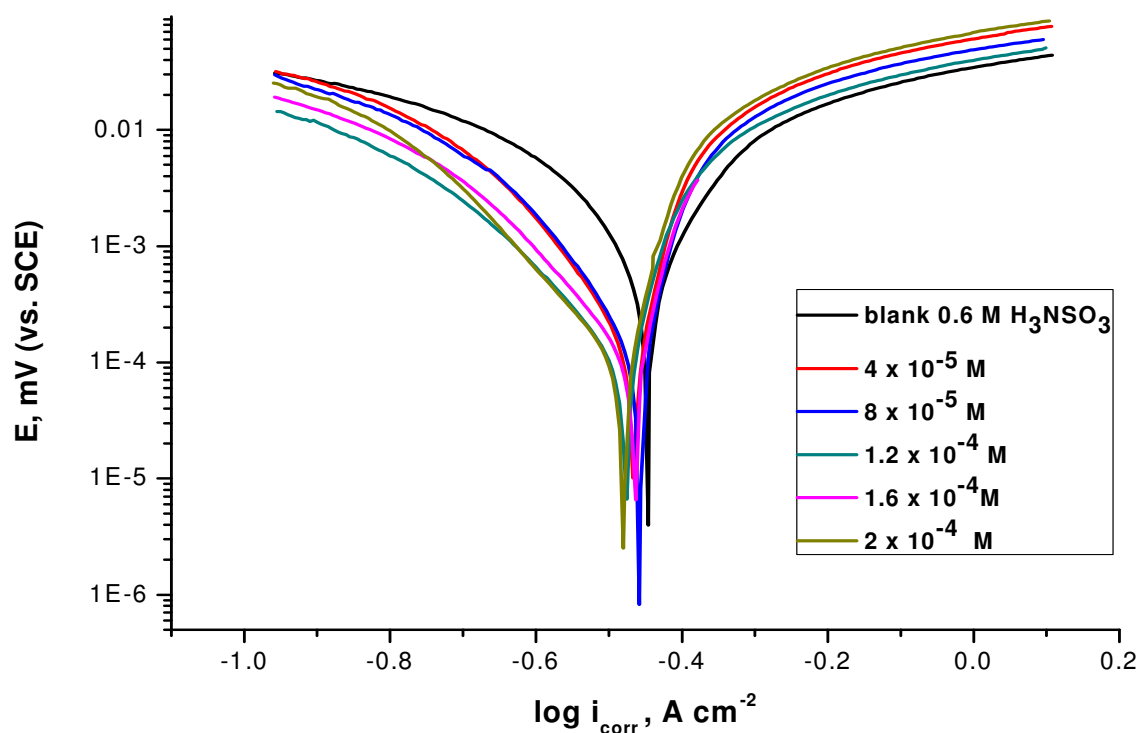


Figure-5

Potentiodynamic polarization curves for the dissolution of 316SS in 0.6 M H₂NHSO₃ in the absence and presence of different concentrations of compound (D) at 25°C

Table-7

Effect of concentrations of various compounds on the free corrosion potential (E_{corr}), corrosion current density (i_{corr}), Tafel slopes (β_c , β_a), corrosion rate (k_{corr}), degree of surface coverage (θ), and inhibition efficiency (%IE) of 316SS in (0.6 M) H_2NHSO_3

Inh	[Inh] $\times 10^5$ M	$-E_{corr}$ mVvsSCE	i_{corr} $\mu A\ cm^{-2}$	β_c mV dec $^{-1}$	β_a mV dec $^{-1}$	k_{corr} mm $^{-1}$	θ	%IE
blank	0.0	446	1160	241	186	1064	--	--
A	4	433	475	179	109	433.9	0.591	59.1
	8	474	261	282	144	238.1	0.775	77.5
	12	480	191	202	107	174.6	0.835	83.5
	16	465	131	150	56	120.1	0.887	88.7
	20	466	95.4	135	53	87.2	0.918	91.8
B	4	436	362	186	107	330.6	0.688	68.8
	8	456	233	176	88	212.8	0.799	79.9
	12	457	189.0	184	79	172.9	0.837	83.7
	16	463	131.0	180	78	119.3	0.887	88.7
	20	477	93.6	145	49	85.5	0.919	91.9
C	4	448	500.0	109	83	457.4	0.569	56.9
	8	460	272.0	225	114	248.9	0.766	76.6
	12	473	192.0	205	93	175.9	0.834	83.4
	16	464	126.0	163	55	114.9	0.891	89.1
	20	472	106.0	147	54	97.0	0.909	90.9
D	4	466	292.0	190	97	266.6	0.748	74.8
	8	459	206.0	162	83	188.4	0.822	82.2
	12	475	159.0	202	79	144.9	0.863	86.3
	16	464	126.0	163	55	114.9	0.891	89.1
	20	480	91.0	141	46	83.2	0.922	92.2

Electrochemical Impedance Spectroscopy Measurements: Nyquist plots of 316SS in uninhibited and inhibited acid solutions containing different concentrations of compound (D) are presented in figure-6. EIS spectra obtained consists of one depressed capacitive loop (one time constant in Bode-phase plot). The increased diameter of capacitive loop obtained in 0.6 M H_2NHSO_3 in presence of compound(D) indicated the inhibition of corrosion of 316SS. The high frequency capacitive loop may be attributed to the charge transfer reaction. Corrosion kinetic parameters derived from EIS measurements and inhibition efficiencies are given in table-8. Double layer capacitance (C_{dl}) and charge transfer resistance (R_{ct}) were obtained from EIS measurements as described elsewhere⁴¹. It is apparent from table 8 that the impedance of the inhibited system amplified with the inhibitor the C_{dl} values decreased with inhibitor. This decrease in C_{dl} results from a decrease in local dielectric constant and/or an increase in the thickness of the double layer, suggested that inhibitor molecules inhibit the iron corrosion by adsorption at the metal/acid interface⁴². The depression in Nyquist semicircles is a feature for solid electrodes and often referred to as frequency dispersion and attributed to the roughness and other inhomogeneities of the solid electrode⁴³. In this behavior of solid electrodes, the parallel network: charge transfer resistance-double layer capacitance is

established where an inhibitor is present. For the description of a frequency independent phase shift between an applied potential and its current response, a constant phase element (CPE) is used which is defined in impedance representation as in equation (5)

$$Z_{CPE} = Y_o^{-1}(i\omega)^{-n} \quad (5)$$

where, Y_o is the CPE constant, ω is the angular frequency (in rad s^{-1}), $i^2 = -1$ is the imaginary number and n is a CPE exponent which can be used as a gauge of the heterogeneity or roughness of the surface⁴⁴. Depending on the value of n , CPE can represent resistance ($n = 0$, $Y_o = R$), capacitance ($n = 1$, $Y_o = C$), inductance ($n = -1$, $Y_o = L$) or Warburg impedance ($n = 0.5$, $Y_o = W$).

Figure-7 showed the electrical equivalent circuit employed to analyze the impedance spectra. Excellent fit with this model was obtained for all experimental data. The surface coverage (θ) and % IE were calculated using equation 6:

$$\%IE = \theta \times 100 = [1 - (R_{ct}/R_{ct}^{\circ})] \times 100 \quad (6)$$

Where R_{ct} and R_{ct}° are the charge transfer resistances in absence and presence of inhibitor, respectively.

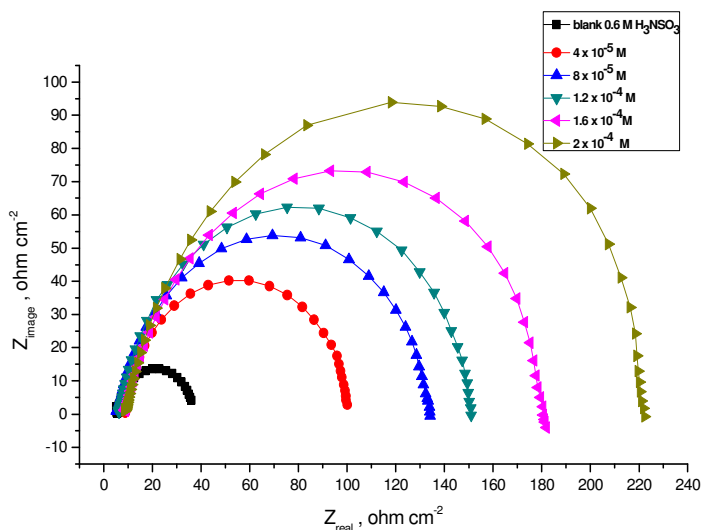


Figure-6

The Nyquist plots for the corrosion of 316SS in 0.6 M H₂NHSO₃ in the absence and presence of different concentrations of compound (D) at 25°C

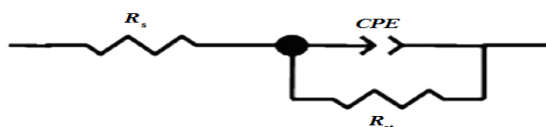


Figure-7

electrochemical equivalent circuit used to fit the impedance measurements that include a solution resistance (R_s), a constant phase element (CPE) and a polarization resistance or charge transfer (R_{ct})

Table-8

EIS parameters for the corrosion of 316SS in 0.6 M H₂NHSO₃ in the absence and presence of different concentrations of investigated compound at 25°C

Inhibitor	Conc. x 10 ⁵ M	C _{dl} μF cm ⁻²	R _{ct} Ω cm ²	θ	%IE
Blank	0.0	452.33	31.57	---	---
A	4	91.23	66.61	0.52	52.6
	8	85.02	124.0	0.74	74.5
	12	53.84	128.8	0.75	75.5
	16	47.18	163.4	0.80	80.7
	20	45.98	200.5	0.84	84.3
B	4	305.47	72.28	0.563	56.3
	8	237.07	117.50	0.731	73.1
	12	109.09	140.00	0.775	77.5
	16	90.75	172.00	0.816	81.6
	20	75.10	210.00	0.850	85.0
C	4	116.72	37.46	0.157	15.7
	8	92.14	116.40	0.729	72.9
	12	90.09	135.00	0.766	76.6
	16	84.88	177.20	0.822	82.2
	20	80.07	206.10	0.847	84.7
D	4	107.07	92.41	0.658	65.8
	8	93.15	130.70	0.758	75.8
	12	90.61	147.20	0.786	78.6
	16	72.99	178.80	0.823	82.3
	20	67.93	224.70	0.860	86.0

The results obtained from weight loss, potentiodynamic polarization and impedance techniques are in a good agreement but it is of interest to note that, the values of % IE given by electrochemical techniques are higher than those obtained by weight loss measurements; this may be due to the fact that the electrochemical measurements were carried out on freshly prepared solutions.

Electrochemical Frequency Modulation Measurements: EFM is a nondestructive corrosion measurement like EIS; it is a small signal ac technique. Unlike EIS, however, two sine waves (at different frequencies) are applied to the cell simultaneously. The great strength of the EFM is the causality factors which serve as an internal check on the validity of the EFM measurement⁴⁵. With the causality factors the experimental EFM data can be verified. The results of EFM experiments are a spectrum of current response as a function of frequency. The spectrum is called the intermodulation spectrum. The spectra contain current responses assigned for harmonical and intermodulation current peaks. The larger peaks were used to calculate the corrosion current. The inhibition efficiencies, % IE calculated from equation 3 increase with increasing the studied inhibitor concentrations. The two frequencies may not be chosen at random. They must both be small, integer multiples of

a base frequency that determines the length of the experiment. Intermodulation spectra obtained from EFM measurements were constructed for iron 0.6 M H_2NHSO_3 solutions as a function of 2×10^{-4} M of compound (D) at 25°C. Each spectrum is a current response as a function of frequency; data not shown here. Corrosion kinetic parameters, namely corrosion current density (i_{corr} , Tafel constants (β_a, β_c) and causality factors (CF-2, CF-3) were listed table-8 as a function of concentrations of investigated compounds at 25°C. The causality factors in table-8, which are very close to theoretical values according to the EFM theory, should guarantee the validity of Tafel slopes and corrosion current densities. The standard values for CF-2 and CF-3 are 2.0 and 3.0, respectively⁴⁶.

Conclusion

In this study, corrosion inhibition efficiency of Oxazole derivatives on in 316SS in 0.6 M H_3NSO_3 was determined by chemical and electrochemical measurements. Electrochemical impedance spectroscopy data reveals increase in R_{ct} values, which accounted for good inhibition efficiency. The polarization studies showed that these compounds behave as mixed type inhibitors. These compounds adsorbed on SS surface followed Langmuir adsorption isotherm.

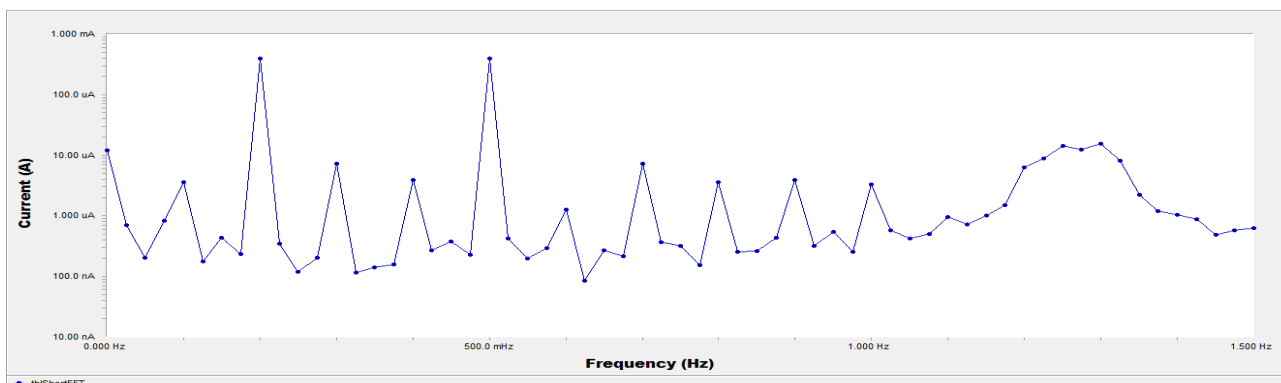


Figure-8
EFM spectra for 316SS in 0.6 M H_3NSO_3 (blank)

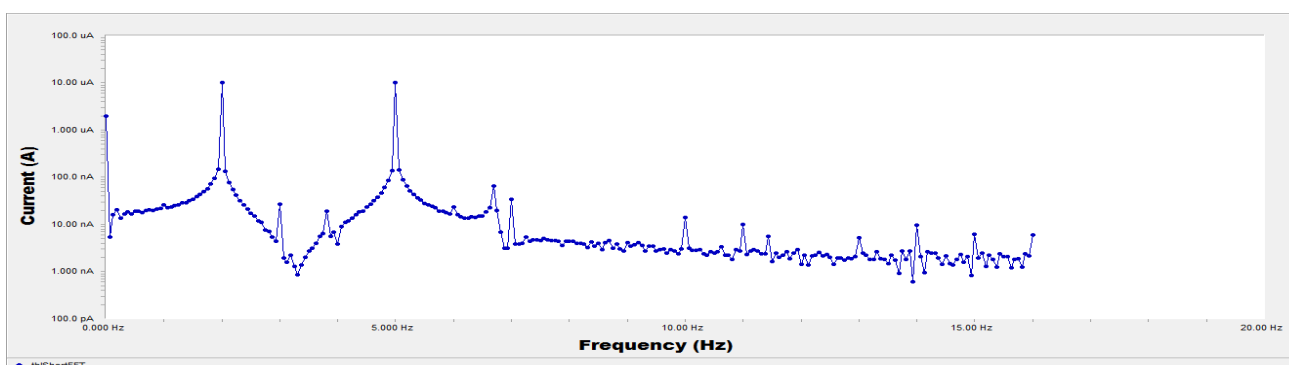


Figure-9
EFM spectra for 316SS in 0.6 M H_3NSO_3 in the presence of 2×10^{-4} M inhibitor (D)

Table-9
Electrochemical kinetic parameters obtained from EFM technique for 316SS in (0.6 M) H₃NSO₃ in the absence and presence of different concentrations of investigated compound.

Inh.	Conc. M	$i_{corr.}$, $\mu A cm^{-2}$	β_a , $mV dec^{-1}$	β_c , $mV dec^{-1}$	CF-2	CF-3	%IE
Blank	0.0	666.0	104	117	2.012	4.579	--
A	4×10^{-5}	297.3	90	112	1.957	3.000	55.4
	8×10^{-5}	173.9	73	122	2.016	2.872	73.9
	1.2×10^{-4}	145.6	63	126	1.952	2.134	78.1
	1.6×10^{-4}	138.4	72	137	1.973	2.859	79.2
	2×10^{-4}	124.0	81	144	1.973	2.830	81.4
B	4×10^{-5}	275.6	105	140	1.984	3.392	58.6
	8×10^{-5}	161.8	59	136	1.942	3.009	75.7
	1.2×10^{-4}	137.4	62	122	1.898	3.236	79.4
	1.6×10^{-4}	135.4	73	158.4	1.965	2.956	79.7
	2×10^{-4}	116.8	70	155	1.953	2.936	82.5
C	4×10^{-5}	322.5	98	116	1.961	2.151	51.6
	8×10^{-5}	228.2	88	145	1.962	4.086	65.7
	1.2×10^{-4}	164.7	74	136	2.000	2.771	75.3
	1.6×10^{-4}	159.2	85	115	1.981	3.138	76.1
	2×10^{-4}	128.4	68	133	1.966	2.801	80.7
D	4×10^{-5}	214.3	88	110	1.917	2.9	67.8
	8×10^{-5}	144.0	71	126	1.965	2.842	78.4
	1.2×10^{-4}	129.0	74	119	1.981	3.089	80.6
	1.6×10^{-4}	116.0	69	142	1.957	3.183	82.6
	2×10^{-4}	59.36	70	198	3.455	2.75	91.0

References

- Malik A.U., Andijani I.N., Siddiqi N.A., Ahmed S. and Al-Mobayaed A.S., studies on the role of sulfamic acid as a desalant in desalination plants, *Technical Report No. SWCC RDC)-32 in (1993)*
- 2. Encyclopedia of chemical technology, Wiley Interscience Publication, 21, 951-57 (1983)*
- Process Industries, *NACE Publication 267-268 (1986)*
4. Metal Hand Book, Corrosion, Specific Industries and Environments, *American Society of Metals, 13, 1140-11 (1987)*
5. Sun J., Yan C.G. and Han Y, *Synth Commun., 31(1) 151-154 (2001)*
- Szocs E., Vastag G. Y., Shabanand A., Kalman E., *Corros. Sci., 47, 893 (2005)*
- Subramanian R., Lakshminarayanan V., *Corros. Sci., 44, 535 (2002)*
- Ramesh S. and Rajeswari S., *Corros. Sci., 47, 151 (2005)*
- El-Naggar M.M., *Corros. Sci, 42, 773 (2002)*
- Zhong D., Gao L., Zhou G., *Corros. Sci., 46, 3031 (2004)*
- Baartly J., Huynh N., Bottle S.E., Flitt H., Notoya T. and Schweinsberg D.P., *Corros. Sci., 45, 81 (2003)*
- Bastidas J. M., Pinilla P., Cano E., Polo J. L. and Miguel S., *Corros. Sci., 45, 427 (2003)*
- Huynh N., Bottle S.E., Notoya T. and Schweinsberg D.P., *Corros. Sci., 44, 2583 (2002)*
- Stupnisek-Lisac E., Brnada A. and Maance A.D., *Corros. Sci. 42, 243 (2000)*
- Moretti G. and Guidi F., *Corros. Sci., 44, 1995 (2002)*
- Szklarska -Smialowska Z., Kaminski M., *Corros. Sci., 13, 1 (1973)*
- Talai J. D., Gandhi D. K., *Corros. Sci., 23, 1315 (1983)*
- Fouda A.S., *Monat. Chem., 117, 159 (1986)*
- Adeyemi O.O. and Singh C., *Bull. Electrochem., 8, 581 (1992)*
- Kandy A.A.S., Al-Oubi A.O., Khalil R.M., Abdel Fattah A.A., *Electrochem., 17, 111 (2001)*
- Mernari B., El Kadi L., Kertit S., *Bull. Electrochem., 17, 115 (2001)*
- Bouklah M., Hammouti B., Aouniti A., Benhadda T., *Prog. Org. Coat., 49, 225 (2004)*
- Galal A., Atta N. F. and Hassan M. H., *Mater. Chem. Phys., 89, 28-37 (2005)*
- Khaled K. F., *J. Appl. Electrochem., 39, 429-438 (2009)*

25. SahinM., Bilgic S. and Ylmaz H., *Appl. Surf. Sci.*, **195**, 1 (2002)
26. ZaafaranyA. and AbdallahM., *Electrochem. Sci.*, **5**, 18-28 (2010)
27. LiX. and MuG., *Appl. Surf. Sci.*, **252**, 1254 (2005)
28. Ameh P.O. and Eddy N.O., Commiphorapedunculata gum as a green inhibitor for the corrosion of aluminum alloy in 0.1 M HCl. *Res. Chem. Intermediates*, 1-9 (2013)
29. Petchiammal A, Deepa RP, Selvaraj S, Kalirajan K. Corrosion Protection of Zinc in Natural Sea Water using Citrullus Vulgaris peel as an Inhibitor, *Res. J. Chem. Sci.*, **2(4)**, 24-34 (2012)
30. FoudaA. S., Al-Sarawy A. A.,El-KatoriE.E, Pyrazolone derivatives as corrosion inhibitors for Carbon steel in hydrochloric acid solution, *Desalination*, 201, 1-13 (2006)
31. Gece G., The use of quantum chemical methods in corrosion inhibitor studies, *Corros. Sci.*, **50**, 2981-2992 (2008)
32. Tang L., LieX., SiY., MuG. and LiuG., *Mater. Chem. Phys.*, **95**, 29 (2006)
33. Tang L., Murad G. and LiuG., *Corros. Sci.*, **45**, 2251 (2003)
34. PutilovaI. N., Balzin S.A. and Barannik V.P., Metallic corrosion Inhibitors, *Pergamomon Press*, 31 (1960)
35. Khamis E., *Corrosion (NACE)* **46**, 476 (1990)
36. LiX. and TangL., *Mater. Chem. Phys.*, **90**, 286 (2005)
37. El-AwadyA. A., Abd El-NabeyB. and AzizS. G., *Electrochem. Soc.*, **139**, 2149 (1992)
38. Abd El-RehimS. S., HassanH. H. and AminM. A., *Mater. Chem. Phys.*, **70**, 64 (2001)
39. SinghA. K., QuraishiM. A., *Corros. Sci.*, **52**, 1373-1385 (2010)
40. BentissF., JamaC., MernariB., AttariH. E., KadiL. E., Lebrini M., Traisnel M., Lagrenee M., *Corros. Sci.*, **51**, 1628-1635 (2009)
41. Ashassi-Sorkhabi H., Seifzadeh D., Hosseini M.G., *Corros. Sci.*, **50**, 3363-3370, *Int. J. Electrochem. Sci.*, Vol. 9, 2014 364 (2008)
42. Popova A. and Christov M., *Corros. Sci.*, **48**, 3208-3221 (2006)
43. GamryEchem Analyst Manual, (2003)
44. Bosch R.W., Hubrecht J., Bogaerts W.F., Syrett B.C., A New Electrochemical Technique for Online Corrosion Monitoring *Corrosion*, **57**, 60 (2001)
45. Abdel-RehimS.S., KhalidK.F., Abd-ElshafiN.S., *Electrochem. Acta*, **51**, 3269-3277, (2006)
46. SinghA. K., Quraishi M. A., *J. Mater. Environ. Sci.*, **1**, 101-110 (2010)